Quantum Electronics **49** (8) 779–783 (2019)

X-RAY SPECTROMETER

https://doi.org/10.1070/QEL17018

Scanning spectrometer/monochromator for a wavelength range of 50–330 Å

A.N. Shatokhin, E.A. Vishnyakov, A.O. Kolesnikov, E.N. Ragozin

Abstract. **A flat-field scanning spectrometer/monochromator of the Hettrick–Underwood type is implemented for a wavelength range $\lambda \approx 50$–330 Å. The optical arrangement of the spectrograph comprises a focusing spherical (R = 6000 mm) mirror, mounted at a grazing angle of 8.34°, and a grazing-incidence plane varied line-space (VLS) grating operating for a constant deflection angle of 16.68°. The entrance and output slits of the instrument are immobile, and the focal distance varies only slightly over its operating spectral range. The short-wavelength boundary of the operating range is determined by the spectral source brightness and the reflection coefficients of the grating and the mirror rather than by defocusing. Laser-produced plasma spectra excited by a focused laser beam (0.5 J, 8 ns, 1.06 μm) are recorded. A spectral resolving power $\lambda/\delta\lambda$ = 1300 is demonstrated at a wavelength of 182 Å. The configuration of the instrument of this type is suited to soft X-ray reflectometry and metrology with the use of laser-plasma and synchrotron radiation sources, and is perfectly compatible with modern CCD detectors.**

Keywords: *soft X-ray radiation, scanning spectrometer, focusing mirror, VLS grating, laser-produced plasma.*

1. Introduction

Vacuum ultraviolet and soft X-ray radiation is extensively used in the study of laboratory and astrophysical plasmas [1–6], in the investigation of new structures, compounds and composites by APRES [7] and absorption spectroscopy (NEXAFS, EXAFS, XANES) [8] techniques, in the spectroscopy of molecules, materials and biological objects by resonant inelastic X-ray scattering (RIXS) technique [9, 10], etc. The sources of this radiation may be traditional (astrophysical and laboratory plasma, including laser-produced microplasma) as well as newest, in which soft X-ray radiation is produced under highly sophisticated conditions: for instance, in a free-electron laser [11] or in the reflection of an IR femtosecond pulse from the relativistic 'flying mirror' produced by a multiterawatt laser pulse in a helium jet [12]. In the latter case, the soft X-ray radiation emerges due to the frequency up-conversion in the double relativistic Doppler effect.

A.N. Shatokhin, A.O. Kolesnikov P.N. Lebedev Physical Institute, Russian Academy of Sciences, Leninsky prosp. 53, 119991 Moscow, Russia; Moscow Institute of Physics and Technology (State University), Institutskii per. 9, 141701 Dolgoprudnyi, Moscow region, Russia; e-mail: shatohinal@gmail.com;
E.A. Vishnyakov, E.N. Ragozin P.N. Lebedev Physical Institute, Russian Academy of Sciences, Leninsky prosp. 53, 119991 Moscow, Russia

Received 19 March 2019; revision received 15 May 2019
Kvantovaya Elektronika **49** (8) 779–783 (2019)
Translated by E.N. Ragozin

The progress of soft X-ray spectroscopy observed in recent years is largely due to the intensive development of new X-ray optical components. In particular, several past decades have seen the development of periodic and aperiodic multilayer mirrors (see, for instance, reviews [13, 14]), free-standing multilayer polarisers, absorption filters, phase-shifting components, etc. Both purely scientific research problems and physicotechnical metrological tasks of characterising X-ray optical elements and calibrating detectors call for the development of convenient spectrometers/monochromators that are specially oriented for solving these tasks and take into account the nature of the radiation source (the source position and the source–spectrometer distance, the radiation divergence, its reproducibility in space and intensity). For reflectometry/metrology tasks, as a rule, use is made of laser plasma (LP) [15] and synchrotron radiation (SR) [16]. As is known from the literature, a LP radiation source is capable of providing an absolute measuring accuracy at a level of ~1%, while SR at a level of ~0.1% due to the high stability of SR.

Hettrick and Underwood [17] proposed a convenient configuration of a high-resolution scanning monochromator, in which the entrance and output slits are immobile, the deflection angle is constant, and scanning is performed by rotating a plane varied line-space (VLS) grating. The grating is illuminated with the converging beam produced by a grazing-incidence focusing mirror. In this case, the spectral meridional image of the entrance slit is strictly at the output slit for two wavelengths (for two rotation angles of the VLS grating), and the departure of the spectral focus from the immobile slit and the defocusing are insignificant throughout a broad wavelength range. Therefore, the Hettrick–Underwood monochromator is perfectly suited to the solution of metrological problems in a broad wavelength range.

The objective of our work is to develop a compact high-resolution laboratory spectrometer and test it by recording the line spectra excited in a LP. The spectrometer made use of a plane VLS-grating, which had been initially designed for an imaging spectrograph comprising a normal-incidence aperiodic mirror for aberration compensation in a broad spectral range [18, 19]. The implementation of this imaging spectrograph provided a spectral resolving power of ~1000 in the 125–250 nm range simultaneously with a spatial resolution of 26 μm [20–22].

2. Optical configuration of the scanning spectrometer/monochromator

Figure 1 displays the optical configuration of the spectrometer. A focusing mirror produces the horizontal focal image of the entrance slit behind the VLS grating at a distance r from its centre. When the instrument operates as a monochromator, an output slit is placed in lieu of the detector. By the

deflection angle is meant the sum of the grazing angles of incidence and diffraction: $\varphi + \psi$ (see Fig. 1). Use is made of the outside diffraction order. The local groove density in the grating aperture is described by the polynomial $p(w) = p_0 + p_1 w + p_2 w^2 + \ldots$, where p_0 is the line density at the grating centre, coefficient p_1 modifies the spectral focal curve, and coefficients p_2 and p_3 suppress meridional coma and spherical aberration, respectively.

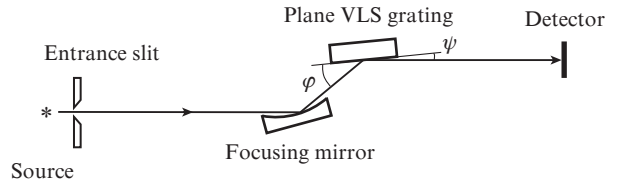

Figure 1. Spectrometer configuration (not to scale). The slit is on the Rowland circle associated with the mirror.

The direction of central ray diffraction is defined by the grating equation

$$\cos\varphi - \cos\psi = mp_0\lambda, \tag{1}$$

and the equation which describes in the paraxial approximation the distance between the horizontal focus of the diffracted beam and the grating is of the form [23, 24]

$$-\frac{\sin^2\varphi}{r} + \frac{\sin^2\psi}{r'_h} = m\lambda p_1. \tag{2}$$

The condition that the focal distance r'_h is constant for the diffracted beam may be fulfilled for two wavelengths (λ_1,λ_2) in the VLS-grating rotation and for the invariable distance r to the focus of the initial beam. The coefficient p_1, which is a grating characteristic, is invariable:

$$p_1 = \left[-\frac{\sin^2\varphi_1}{r} + \frac{\sin^2\psi_1}{r'_h}\right]\frac{1}{m\lambda_1} = \left[-\frac{\sin^2\varphi_2}{r} + \frac{\sin^2\psi_2}{r'_h}\right]\frac{1}{m\lambda_2}, \tag{3}$$

and therefore

$$\frac{r'_h}{r} = \frac{\lambda_2\sin^2\psi_1 - \lambda_1\sin^2\psi_2}{\lambda_2\sin^2\varphi_1 - \lambda_1\sin^2\varphi_2}. \tag{4}$$

Considering that $m\lambda_{1,2} = (\cos\varphi_{1,2} - \cos\psi_{1,2})/p_0$, we obtain

$$\frac{r'_h}{r} = \frac{(\cos\varphi_2 - \cos\psi_2)\sin^2\psi_1 - (\cos\varphi_1 - \cos\psi_1)\sin^2\psi_2}{(\cos\varphi_2 - \cos\psi_2)\sin^2\varphi_1 - (\cos\varphi_1 - \cos\psi_1)\sin^2\varphi_2}. \tag{5}$$

One can see from expression (5) that it is possible to fix some incidence angles $\varphi_{1,2}$ and the deflection angle $\varphi + \psi$ (or, which is the same, wavelengths $\lambda_{1,2}$ and p_0) as well as the absolute dimensions of the instrument (coefficient p_1 will be expressed in terms of them using Eqn (3).

Given below are the parameters of the VLS spectrometer realised in our work. For $\lambda_{1,2}$ we selected the wavelengths 140 and 273 Å. The outside diffraction order was selected for the following two reasons. First, in the configuration with a constant deflection angle the passage to shorter wavelengths is made by decreasing the angle φ of grazing incidence on the grating, which permits maintaining the reflection coefficient at a sufficiently high level. Second, to the outside diffraction order there corresponds a stronger dispersion, which permits realising a higher practical resolving power in view of the finite size of the CCD detector pixels (13.5 μm).

Radius of curvature of spherical mirror/mm	6000
Diameter of spherical mirror/mm	60
Grazing angle of incidence on the mirror equal to half the grating deflection angle/deg	8.34
Distance between mirror and grating centres/mm	336.7
Entrance slit – mirror distance/mm	870.4
Dimensions of 'ruled' grating area/mm	50 × 25
Rigorous focusing wavelength λ_1/Å	140
Angle φ_1 of incidence on the grating corresponding to λ_1/deg	10
Diffraction angle ψ_1 corresponding to λ_1/deg	6.68
Rigorous focusing wavelength λ_2/Å	273
Angle φ_2 of incidence on the grating corresponding to λ_2/deg	11.58
Diffraction angle ψ_2 corresponding to λ_2/deg	5.10
Grating – detector distance/mm	532.6
Distance of converging beam focus from the grating/mm	533.7
Groove density p_0 at VLS-grating aperture centre/mm^{-1}	600
Coefficient p_1/mm^{-2}	2.22
Coefficient p_2/mm^{-3}	6×10^{-3}
Plate scale at wavelength λ_1/Å mm^{-1}	3.64
Plate scale at wavelength λ_2/Å mm^{-1}	2.78
Resolving power at wavelength λ_1 corresponding to the size of one CCD detector pixel (13.5 μm)	3000

Figure 2 displays the shape of the focal curve (the dotted line) for different grating rotation angles corresponding to wavelengths of 100, 140, 180, 220, 260, and 274 Å in the direction of the detector centre (or the output slit). This direction is shown with a bold horizontal line, which coincides with the central ray of the diffracted beam. Thin lines serve to indicate the course of the rays corresponding to other wavelengths for the given grating rotation angle. The grating rotation angle is measured from the position, whereby $\varphi = \psi$ and the zero diffraction order arrives at point D. The detector plane is centred at point D and is shown with a dashed vertical line segment of length 27 mm. The focal curve intersects point D at wavelengths $\lambda_1 = 140$ Å and $\lambda_2 = 273$ Å. In the monochromator mode (the output slit is at point D) the focal image–slit distance does not exceed 0.6 mm, which results in image defocusing of less than 6 μm (half the detector pixel size) in the 100–300 Å range. In the calculation of the position of the paraxial focus in Fig. 2 we used formulas (2) and (1), the angle φ being equal to the sum of 8.34° and the grating rotation angle. The image of the entrance slit produced by the mirror served as the imaginary source in formula (2).

For fixed VLS-grating rotation angles the spectral focal curve has a small curvature and may be approximated with a straight-line segment in a rather broad spectral interval, and so the configuration may be treated as a scanning flat-field spectrometer. Furthermore, in this case the angle between the

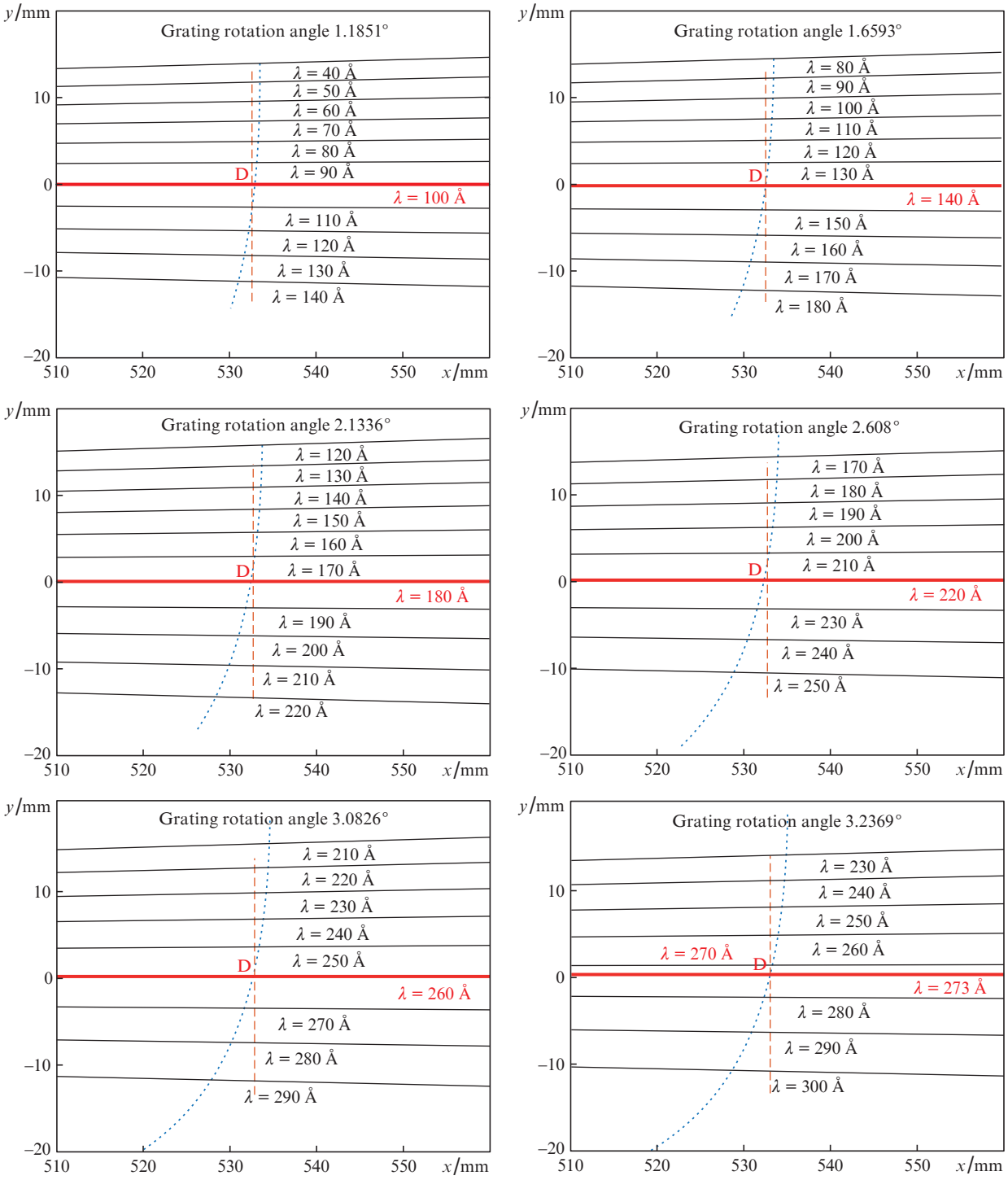

Figure 2. Paths of the rays and of the focal curve (dotted line) for different grating rotation angles. The distance from the VLS-grating centre is plotted on the x axis. Plotted on the y axis is the distance measured from the central ray in the perpendicular direction (along the dispersion direction).

central diffracted ray and the focal curve is close to 90°, which makes this scheme perfectly compatible with modern CCD detectors.

In the spectrometer mode, for all grating rotation angles the focusing persists in an interval of several tens of angstroms when the plane of the sensitive detector surface is perpendicular to the central ray of diffracted beam. Since the focal curve is not exactly perpendicular to the central ray, in the spectrometer mode it is expedient to rotate the detector by a small (approximately 3°–5°) angle to broaden the interval of 'good' focusing (for a fixed VLS-grating rotation angle) to about 100 Å.

The scanning spectrometer mode is convenient for recording a relatively narrow selected portion of the spectrum with a high resolution. An example is provided by the group of the C VI ion Balmer lines 4 → 2 (135 Å), 5 → 2 (120.5 Å) and 6 → 2 (114 Å), which is suited for measuring the electron plasma density from the Stark line broadening. In this case, the scan-

ning spectrometer mode offers an indisputable advantage over the monochromator mode, especially so in the operation with pulsed sources characterised by a moderate reproducibility of its spectra. Therefore, a virtue of the scanning spectrometer is the capability of a detailed (with a strong dispersion) examination of the spectral interval selected from the operating spectral range about two octaves in width.

Plotted in Fig. 3 is the width of the image of a point source arising from the geometrical defocusing during wavelength scanning. By the geometrical defocusing is meant the spectral image broadening caused by the departure of the focal curve from the detector position. It is equal to the product of the focus–detector distance and the convergence angle of diffracted beam. As suggested by the spectral images of a point monochromatic source obtained by numerical ray tracing, the geometric defocusing makes the main contribution to the broadening of the spectral images. At the points of exact focusing ($\lambda_1 = 140$ Å and $\lambda_2 = 273$ Å), the residual image width is determined by meridional coma and spherical aberration, as well as by the beam diffraction, and does not exceed the detector pixel size. One can see that the width of the image of a point source does not exceed the size of detector pixels in the wavelength range $\lambda < 330$ Å. This signifies that the practical short-wavelength bound of the operating spectral range is limited only by the mirror and VLS-grating reflectivities as well as by the source brightness. The maximal acceptance angle is defined by the grating width and is wavelength-dependent.

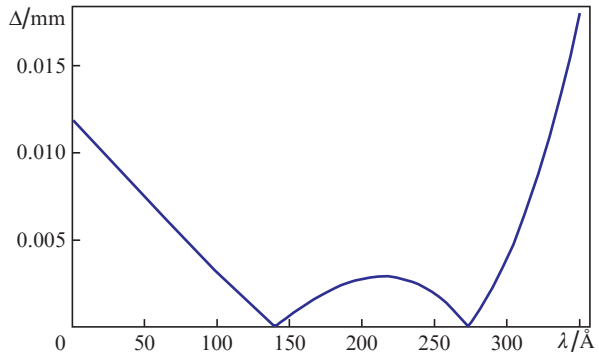

Figure 3. Width Δ of the image of a point source caused by geometrical defocusing in the scanning over the source wavelength (the detector is immobile).

The quality of focusing was verified using numerical ray tracing to construct the spectral images of a point source at different wavelengths. In doing this the correctness of analytical calculations was borne out.

3. Spectrometer operation

The VLS grating was made by interference lithography technique in the Scientific and Production Association 'State Institute of Applied Optics' (Kazan). Gold reflective coatings were deposited on the spherical mirror and the VLS grating. The radiation was recorded with a Greateyes (Germany) CCD detector array (2048 × 512 pixels). The spectrometer components were mounted and aligned on a two-metre optical bench, after which the spectrometer was accommodated in a vacuum chamber (3.8 × 0.9 m). The grating was placed on a motorised rotation stage and the detector on a motorised translation stage, which made it possible to carry out the final in-vacuum alignment of the configuration when recording the line spectra of LP. The spectrometer was tested in the recording of the line spectra of multiply charged ions excited by neodymium laser pulses (0.5 J, 8 ns, 1.06 μm).

Figure 4 shows a panoramic magnesium-plasma spectrogram obtained by 'stitching' together ten spectrograms obtained for different VLS-grating rotation angles. The panoramic spectrum is given merely as an example to demonstrate the high spectral resolving power of the instrument in a broad spectral range. The angular magnification of the configuration depends on the grating rotation angle and varies from 1.5 (for $\lambda = 140$ Å) to 2.3 (for $\lambda = 273$ Å). At these wavelengths the image of the entrance slit is therefore projected onto strips that are 1.5 and 2.3 times broader than the initial slit width. The resolving power does not become lower when the slit is projected onto one detector pixel (13.5 μm), i.e. its width for these wavelengths must be equal to about 9 and 6 μm, respectively. In this case, the spectral resolving power is defined by the spatial detector resolution and amounts to several thousand.

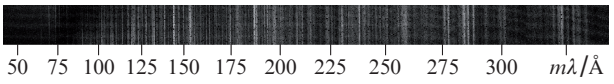

Figure 4. Panoramic spectrogram of magnesium plasma. The 30-μm wide entrance slit was imaged onto the detector in stripes of width 45 and 70 μm in the short-wavelength ($\lambda_1 = 140$ Å) and long-wavelength ($\lambda_2 = 273$ Å) parts of the spectrum, respectively, which was three-five times the optimal width. The linewidths and resolvable line pairs testify to an instrument resolving power of ~ 1000.

Figure 5 displays a portion of the plasma spectrum obtained in the irradiation of a LiF target. Figure 6 shows the profile of the H_α C VI ion line, which demonstrates the fine structure of the line; in this case, the resolving power amounts to 1300. To reduce the Doppler broadening and observe the fine structure, the LP source was displaced from the spectrometer axis, so that the acceptance angle of the spectrometer viewed only the edge of the ion expansion cone, for which

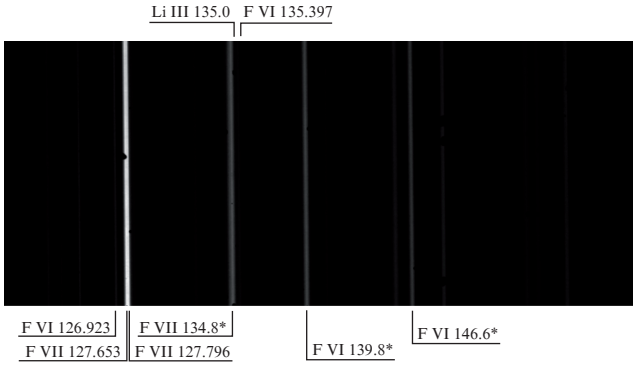

Figure 5. Portion of the plasma spectrum recorded in the irradiation of a LiF target. Unresolved line groups are indicated with an asterisk (*).

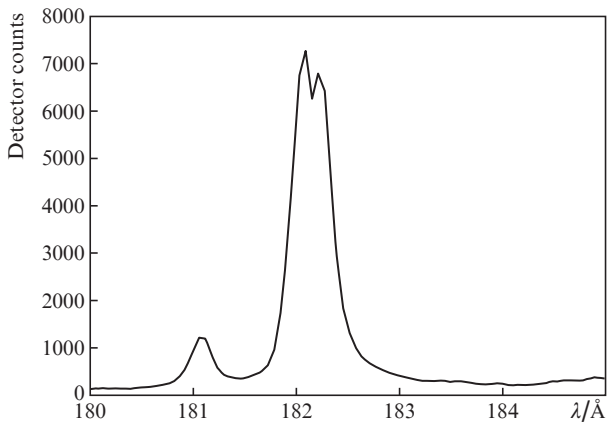

Figure 6. Profile of the Balmer line H_α of C VI ions. The resolved fine structure (0.14 Å) of the line testifies to a resolving power of 1300 in this spectral region. The width of the entrance slit is equal to 10 μm. An unresolved group of oxygen lines is seen in the 181 Å region.

the Doppler broadening in the axial direction was smaller than for the central plasma domain.

4. Conclusions

We have designed and implemented a scanning VLS spectrometer/monochromator of the Hettrick–Underwood type for a wavelength range of 50–330 Å. The spectrometer comprises a grazing-incidence spherical mirror and a grazing-incidence plane VLS grating, which operates in the outside diffraction order. The spectrometer was tested by recording the line spectra from laser-produced plasma, and a spectral resolving power of 1300 was demonstrated at a wavelength of 182 Å.

Two instrument operating modes are possible. In the monochromator mode it may be used for the purposes of metrology and reflectometry, for instance, in combination with a synchrotron or laser-plasma radiation source. In this case, wavelength scanning is performed by rotating the grating, the remaining elements, including the source and the output slit, being immobile.

In the scanning spectrometer mode, the instrument is intended for a detailed (with a strong dispersion and, accordingly, a high spectral resolution) examination of the portion of a spectrum selected from the spectral operating range approximately two octaves in width. Among the possible applications of the instrument is the measurement of linewidths and relative line intensities, including in the operation of pulsed sources with a poor reproducibility of emission spectrum.

Acknowledgements. This work was supported by the Russian Science Foundation (Project No. 14-12-00506).

References

1. Pirozhkov A.S., Kando M., Esirkepov T.Zh., et al. *Phys. Rev. Lett.*, **108**, 135004 (2012).
2. Ragozin E.N., Mednikov K.N., Pertsov A.A., Pirozhkov A.S., Reva A.A., Shestov S.V., Ul'yanov A.S., Vishnyakov E.A. *Proc. SPIE Int. Soc. Opt. Eng.*, **7360**, 73600N (2009).
3. Beigman I.L., Levashov V.E., Mednikov K.N., Pirozhkov A.S., Ragozin E.N., Tolstikhina I.Yu. *Quantum Electron.*, **37** (11), 1060 (2007) [*Kvantovaya Elektron.*, **37** (11), 1060 (2007)].
4. Beigman I.L., Vishnyakov E.A., Luginin M.S., Ragozin E.N., Tolstikhina I.Yu. *Quantum Electron.*, **40** (6), 545 (2010) [*Kvantovaya Elektron.*, **40** (6), 545 (2010)].
5. Kuzin S.V., Zhitnik I.A., Shestov S.V., et al. *Solar Syst. Res.*, **45** (2), 162 (2011).
6. Shestov S., Reva A., Kuzin S. *Astrophys. J.*, **780** (1), 15 (2014).
7. Strocov V.N., Wang X., Shi M., et al. *J. Synchrotron Rad.*, **21**, 32 (2014).
8. Stöhr J. *NEXAFS Spectroscopy* (Berlin: Springer, 1996).
9. Fuchs O., Weinhardt L., Blum M., et al. *Rev. Sci. Instrum.*, **80**, 063103 (2009).
10. Warwick T., Chuang Yi-De, Voronov D.L., Padmore H.A. *J. Synchrotron Rad.*, **21**, 736 (2014).
11. Louis E., Khorsand A.R., Sobierajski R., et al. *Proc. SPIE*, **7361**, 73610I (2009).
12. Kando M., Pirozhkov A.S., Kawase K., et al. *Phys. Rev. Lett.*, **103** (23), 235003 (2009).
13. Vishnyakov E.A., Kamenets F.F., Kondratenko V.V., et al. *Quantum Electron.*, **42** (2), 143 (2012) [*Kvantovaya Elektron.*, **42** (2), 143 (2012)].
14. Pirozhkov A.S., Ragozin E.N. *Phys. Usp.*, **58** (11), 1095 (2015) [*Usp. Fiz. Nauk*, **185** (11), 1203 (2015)].
15. Gullikson E.M., Underwood J.H., Batson P.C., Nikitin V.J. *X-Ray Sci. Technol.*, **3**, 283 (1992).
16. Underwood J.H., Gullikson E.M., Koike M., Mrowka S. *Proc. SPIE*, **3150**, 40 (1997).
17. Hettrick M.C., Underwood J.H. *AIP Conf. Proc.*, **147**, 237 (1986).
18. Vishnyakov E.A., Shatokhin A.N., Ragozin E.N. *Quantum Electron.*, **45** (4), 371 (2015) [*Kvantovaya Elektron.*, **45** (4), 371 (2015)].
19. Vishnyakov E.A., Kolesnikov A.O., Kuzin A.A., Negrov D.V., Ragozin E.N., Sasorov P.V., Shatokhin A.N. *Quantum Electron.*, **47** (1), 54 (2017) [*Kvantovaya Elektron.*, **47** (1), 54 (2017)].
20. Ragozin E.N., Belokopytov A.A., Kolesnikov A.O., Muslimov E.R., Shatokhin A.N. *Proc. SPIE Int. Soc. Opt. Eng.*, **10235**, 102350L (2017).
21. Vishnyakov E.A., Kolesnikov A.O., Shatokhin A.N., Ragozin E.N. *Proc. SPIE Int. Soc. Opt. Eng.*, **10677**, 106770E (2018).
22. Shatokhin A.N., Kolesnikov A.O., Sasorov P.V., Vishnyakov E.A., Ragozin E.N. *Opt. Express*, **26** (15), 19009 (2018).
23. Vishnyakov E.A., Kolesnikov A.O., Pirozhkov A.S., Ragozin E.N., Shatokhin A.N. *Quantum Electron.*, **48** (10), 916 (2018) [*Kvantovaya Elektron.*, **48** (10), 916 (2018)].
24. Ragozin E.N., Vishnyakov E.A., Kolesnikov A.O., Pirozhkov A.S., Shatokhin A.N. *Aperiodicheskie elementy v optike myagkogo rentgenovskogo diapazona* (Aperiodic Elements in Soft X-Ray Optics). Ed. by E.N. Ragozin (Moscow: Fizmatlit, 2018).